

RESEARCH ARTICLE

10.1002/2014JA019958

Annual fractions of high-speed streams from principal component analysis of local geomagnetic activity

L. Holappa¹, K. Mursula¹, T. Asikainen¹, and I. G. Richardson^{2,3}

Key Points:

- PC analysis is used first time to study long-term geomagnetic activity
- We find that the second PC describes and quantifies the latitudinal differences
- We find that the second PC is related to the annual fraction of high-speed streams

Correspondence to:

L. Holappa,
lauri.holappa@oulu.fi

Citation:

Holappa, L., K. Mursula, T. Asikainen, and I. G. Richardson (2014), Annual fractions of high-speed streams from principal component analysis of local geomagnetic activity, *J. Geophys. Res. Space Physics*, 119, 4544–4555, doi:10.1002/2014JA019958.

Received 21 MAR 2014

Accepted 24 MAY 2014

Accepted article online 29 MAY 2014

Published online 18 JUN 2014

¹ReSoLVE Centre of Excellence, Department of Physics, University of Oulu, Oulu, Finland, ²CRESST/Department of Astronomy, University of Maryland, College Park, Maryland, USA, ³Exploration of the Universe Division, NASA/GSFC, Greenbelt, Maryland, USA

Abstract We study the latitudinal distribution of geomagnetic activity in 1966–2009 with local geomagnetic activity indices at 26 magnetic observatories. Using the principal component analysis method we find that more than 97% of the variance in annually averaged geomagnetic activity can be described by the two first principal components. The first component describes the evolution of the global geomagnetic activity, and has excellent correlation with, e.g., the *Kp*/*Ap* index. The second component describes the leading pattern by which the latitudinal distribution of geomagnetic activity deviates from the global average. We show that the second component is highly correlated with the relative (annual) fraction of high-speed streams (HSS) in solar wind. The latitudinal distribution of the second mode has a high maximum at auroral latitudes, a local minimum at subauroral latitudes and a low maximum at midlatitudes. We show that this distribution is related to the difference in the average location and intensity between substorms related to coronal mass ejections (CMEs) and HSSs. This paper demonstrates a new way to extract useful, quantitative information about the solar wind from local indices of geomagnetic activity over a latitudinally extensive network.

1. Introduction

Geomagnetic activity, i.e., short-term variation of the Earth's magnetic field, has been studied since the mid-nineteenth century. Geomagnetic activity is due to the interaction between the Earth's magnetic field and the solar wind and the accompanied interplanetary magnetic field (IMF), which drives different current systems in the magnetosphere and the ionosphere. Magnetic disturbances produced by these current systems on the ground have traditionally been characterized by different global geomagnetic indices, such as the *aa*, *Kp*/*Ap*, *AE*, and *Dst* indices. While some of them (e.g., *aa* and *Kp*/*Ap*) aim to evaluate the global level of geomagnetic activity, including contributions from all main current systems, others (e.g., *Dst* and *AE*) aim to concentrate only one current system. (Note, however, that no pure indices of one current system exist, e.g., the *Dst* index includes contributions from magnetopause, tail and field-aligned currents, at least at times). The long time span of geomagnetic measurements and related indices makes them very important for space climate studies since they provide some of the longest measures of solar activity.

While there are numerous papers written on the temporal development of global geomagnetic activity using, e.g., the standard geomagnetic indices such as *aa*, *Kp*/*Ap*, *AE*, and *Dst*, there are only few recent studies on its spatial structure. This is rather surprising since it is obvious that there is more information included in a large set of local geomagnetic indices than in one single global index (normally a weighted average of several local indices). Recently, local indices have been used to study, e.g., the spatial properties of the ring current, which is often very asymmetric in local time [Yakovchouk *et al.*, 2012; Newell and Gjerloev, 2012].

The most severe types of geomagnetic activity, especially substorms and storms, are primarily driven by two types of solar wind structures: coronal mass ejections (CMEs) and high-speed solar wind streams (HSSs) (including the associated corotating interaction regions; CIRs). Probably, the most important difference between these two drivers is their different characteristic IMF B_z profile. During CMEs, there is often a long period of persistently negative B_z , while during CIRs/HSSs B_z is typically fluctuating around zero, and periods of negative B_z are shorter but more frequent and occur over a longer time [see, e.g., Tsurutani *et al.*, 2006]. Consequently, CMEs and CIRs/HSSs drive geomagnetic activity differently. Most intense ($Dst < -100$ nT) geomagnetic storms are produced by CMEs, while CIR-driven storms are typically limited to smaller intensities [Zhang *et al.*, 2007; Richardson *et al.*, 2006], and about 50% of moderate geomagnetic storms (-100 nT $< Dst < -50$ nT) are driven by CIRs/HSSs [Echer *et al.*, 2013]. Due to their longer duration and the embedded

Alfvén waves [Belcher and Davis, 1971], HSSs can produce significant and long-lasting auroral electrojet activity. While it is known that the most extensive aurorae (and the strongest auroral electrojets and ground disturbances) are caused by CMEs [Borovsky and Denton, 2006], HSSs dominate the auroral activity over long time scales. Tanskanen et al. [2005] studied substorms using ground-based magnetograms and found that their yearly averaged occurrences and amplitudes over the solar cycle strongly correlate with the annual means of the solar wind speed dominated by high-speed streams. Thus, substorm activity is dominated by HSSs at the yearly time scale.

The relative abundance of CMEs and HSSs in the solar wind varies over the solar cycle. While the occurrence of the CMEs roughly correlates with the sunspot number, the occurrence of the HSSs typically maximizes later in the declining phase of the solar cycle when polar coronal holes have nonaxisymmetric extensions to lower latitudes. This leads to the well-known fact that global geomagnetic activity typically has a rough double-peak structure during the solar cycle, the first peak broadly around the sunspot maximum being mostly caused by CMEs and the second peak during the declining phase mostly caused by HSSs [Feynman, 1982; Simon and Legrand, 1986; Richardson et al., 2000; Richardson and Cane, 2012].

These differences between HSSs and CMEs lead to differences in the temporal and latitudinal distributions of geomagnetic activity during HSSs and CMEs. Moreover, the latitudinal distribution of geomagnetic activity changes as a function of the solar cycle phase. This raises an interesting question: is it possible to determine the relative fraction of occurrence of the different solar wind drivers from the latitudinal distribution of geomagnetic activity? In this paper, the latitudinal distribution of geomagnetic activity and its temporal evolution are studied using local A_h indices (digital reconstructions of analog A_k indices) [Mursula and Martini, 2007a] at a wide network of magnetic stations over an extended period of time. We will show that the latitudinal distribution of geomagnetic activity is indeed largely controlled by the relative occurrence of HSSs and CMEs in the solar wind. The main purpose of the present study is to develop a method that can be used to gain information about the statistical occurrence of various solar wind structures before the satellite era.

This paper is organized as follows. Section 2 reviews the K -based geomagnetic indices and the A_h index. Section 3 describes the geomagnetic data and solar wind data used in this paper. The analysis of the paper is largely based on the principal component analysis (PCA) method which is described and applied to the A_h indices in section 4. The results of the PCA are discussed in section 5, and final conclusions of the paper are presented in section 6.

2. K -Based Indices and the A_h Index

Geomagnetic indices with the longest time span (aa and Kp/Ap) are based on the K index method [Bartels et al., 1939; Menvielle and Berthelier, 1991]. The K index is defined in 3 h intervals from the range (maximum-minimum) of the horizontal (H) component of the local magnetic field intensity after first removing the quiet-day variation. The ranges are transformed to quasi-logarithmic K values (numbers from 0 to 9) according to conversion tables which are defined separately for each station. The global Kp index is calculated from the local K indices of 13 observatories which are located in geomagnetic latitudes 48.6° – 62.0° in the Northern Hemisphere and 45.6° – 47.2° in the Southern Hemisphere [GFZ Potsdam, 2012]. The Ap index is the linearized version of the Kp index. The longest continuous geomagnetic index is the aa index (starting from 1868) which is defined as an average of the linearized K indices (so-called A_k indices) of two antipodal stations, one in UK and one in Australia [Mayaud, 1972, 1980]. The K -based indices, especially the aa index, have been used in many studies to describe, e.g., the centennial evolution of global geomagnetic activity.

Although K indices have been measured routinely at several stations, there are many more stations whose magnetic field measurements are given in the international data bases as digital hourly values for several decades. In order to be able to use these data for a latitudinally extended network, we have calculated for each station the recently suggested A_h index of local geomagnetic activity [Mursula and Martini, 2007a], which uses a modified K index method and hourly digital magnetic data. The A_h index (A for amplitude, h for hourly), like the K index, is defined in 3 h intervals from the range of the H component after quiet-day variation removal. However, the A_h index is defined simply as the range itself, unlike in the K method in which the ranges are converted to K numbers in a quasi-logarithmic scale. The A_h index is thus more closely related to the linear A_k index and correlates with it very well [Mursula and Martini, 2007a, 2007b]. Hence, A_h indices can be used here to study latitudinal distribution of geomagnetic activity in a consistent way.

Table 1. Stations and Their Coordinates^a

#	Station Name and Code	Geographic Latitude	Geographic Longitude	CGM Latitude	CGM Longitude
1	Alibag (ABG)	18.638	72.872	9.52	145.27
2	MBour (MBO)	14.384	-16.967	20.78	56.717
3	Kanoya (KNY)	31.420	130.882	24.17	202.020
4	Kakioka (KAK)	36.233	140.183	28.78	210.93
5	San Juan (SJG)	18.382	-66.118	29.27	5.02
6	Memambetsu (MMB)	43.907	144.193	36.56	214.56
7	Chambon-la-Foret (CLF)	48.017	2.267	43.67	79.94
8	Irkutsk (IRT)	52.167	104.450	46.78	176.67
9	Belsk (BEL)	51.837	20.792	47.41	96.38
10	Niemegk (NGK)	52.072	12.675	47.93	89.65
11	Hartland (HAD)	51.000	-4.483	47.99	75.55
12	Wingst (WNG)	53.743	9.073	50.05	87.31
13	Fredericksburg (FRD)	38.210	-77.367	50.07	356.16
14	Eskdalemuir (ESK)	55.317	-3.200	52.95	78.22
15	Victoria (VIC)	48.517	-123.417	54.04	294.56
16	Nurmijärvi (NUR)	60.508	24.655	56.69	102.78
17	Lerwick (LER)	60.133	-1.183	58.16	82.11
18	Sitka (SIT)	57.052	-135.335	59.82	278.10
19	Meanook (MEA)	54.615	-113.347	62.41	303.72
20	Sodankylä (SOD)	67.367	26.633	63.64	108.17
21	College (CMO)	64.867	-147.860	64.88	261.68
22	Abisko (ABK)	68.358	18.823	65.11	102.91
23	Leirvogur (LRV)	64.183	-21.7	65.46	68.57
24	Fort Churchill (FCC)	58.786	-94.088	69.61	330.03
25	Baker Lake (BLC)	64.333	-96.033	74.59	324.68
26	Thule (THL)	77.483	-69.167	86.00	36.77

^aStations are ordered according to their corrected geomagnetic (CGM) latitudes.

3. Data

3.1. Hourly Observatory Data

We use in this study hourly data from 26 ground-based magnetic observatories around the world. The criteria for choosing the observatories were the continuity, length, and quality of their data. The observatories and their geographic and (corrected) geomagnetic coordinates are listed in Table 1. The geomagnetic coordinates are calculated according to the International Geomagnetic Reference Field (IGRF) model (epoch 1985) [IGRF, 2010]. All these stations have continuous data (H component) covering at least the years 1966–2009 included in this study. The data were defined continuous if no more than 20% of hourly H values were missing for any year. It is important to have as complete data as possible for every year, because geomagnetic phenomena are seasonally varying, and incomplete data may lead, e.g., to an erroneous yearly average if a large fraction of data is missing. On the other hand, too strict a requirement for completeness of data reduces the number of stations available and therefore reduces the latitudinal coverage of the study.

All magnetic data have been downloaded from the World Data Center of Edinburgh [WDC-C1, 2011]. Data was checked for possible erroneous points (outliers) using the following method [see Karinen and Mursula, 2005]. The data were first filtered by three-point median filter which replaces each data point by the median of the point itself and its two neighboring points. The filtered data were then subtracted from the original data. Standard deviation of this difference was calculated and statistically abnormal data points which differed by more than 20 standard deviations from the average were considered as possible outliers. All outliers were carefully checked before removing any points from the data. For example, the large positive deflections in the H component that frequently precede the main phase of a geomagnetic storm were not considered as outliers. The data were also checked for possible sudden (step-like) changes in the

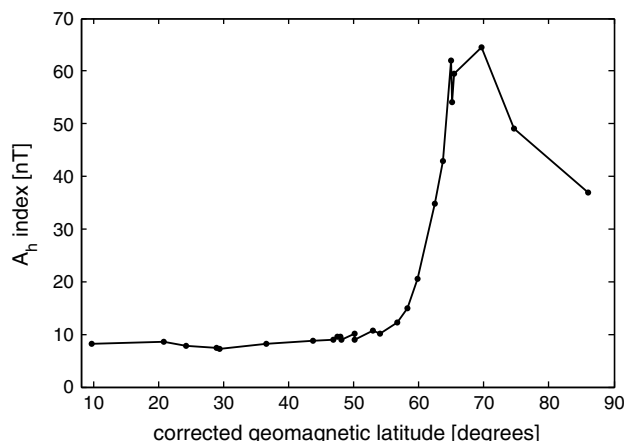


Figure 1. Average values of A_h indices in 1966–2009 as a function of corrected geomagnetic latitude.

baseline (most likely due to erroneous or inconsistent baseline calibration). There were baseline steps in ABG (2 steps), SJG (2), and VIC (1) stations. The steps were corrected by shifting the data before the steps so that the baseline became continuous. A third problem was found in the data of CLF station due to an inhomogeneous sampling method. Hourly values of CLF have been measured as spot values until the end of 1971 and as hourly means since the beginning of 1972. Because of the higher variance of spot values, the A_h index of CLF is excessively large before 1972. The A_h index of CLF was corrected using the method suggested and used in *Martini and Mursula* [2008]. The ratios of the annual averages of A_h indices at CLF and NGK were calculated for years 1962–1971 and 1972–1981 (NGK was selected as a reference station also in *Martini and Mursula* [2008] and is fairly close to CLF in latitude and longitude). The mean values of the ratios are 0.8778 (NGK/CLF in 1962–1971) and 1.0776 (NGK/CLF in 1972–1981). The ratio $0.8778/1.0776 = 0.8146$ was then used to scale down the CLF A_h index in 1966–1971.

3.2. Standardization of A_h Indices

Figure 1 shows the averages of the A_h indices of all the 26 stations over the whole interval 1966–2009 plotted as a function of the corrected geomagnetic latitude. The latitudinal distribution of geomagnetic activity using the A_h index is very similar to that found earlier, e.g., using the *IHV* index [*Svalgaard and Cliver*, 2007]. The average level of geomagnetic activity is rather constant from low latitudes to subauroral latitudes, increases rapidly at about 60° and maximizes at about 67°–70°, which corresponds to the average location of the auroral electrojets. There is almost an order of magnitude difference in average geomagnetic activity between auroral and low latitudes. However, we are not interested now in the absolute level of local geomagnetic activity, or the different source current systems producing this activity, but rather in its variation around its locally averaged level. The A_h indices at auroral latitudes have also much higher variances than the low-latitude indices. In order to guarantee that all stations have equal weight in the analysis, we standardize the indices to unit variance, i.e., we calculate for each station separately the standardized indices

$$A_{hs} = \frac{A_h - \langle A_h \rangle}{\sigma} \tag{1}$$

where $\langle \cdot \rangle$ denotes the mean and σ the standard deviation. The indices are studied both at annual and 3-hourly time scales, when the means and standard deviations are calculated from the annual means or 3-hourly values, respectively. Note also that each local A_h index responds to a variety of current systems by a different weight. Using the standardized A_h indices allows to study relative changes of the net geomagnetic activity across different latitudes.

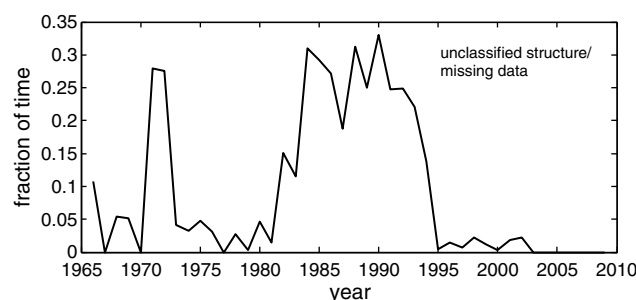


Figure 2. Yearly fraction of gaps (time that is not classified to any SW type) in the list of *Richardson and Cane* [2012].

3.3. Solar Wind Structures

As mentioned earlier, CMEs and HSSs are the two most important drivers of geomagnetic activity. *Richardson et al.* [2000] and *Richardson and Cane* [2012] have divided the solar wind observed at the Earth's orbit since 1963 into three basic types: high-speed streams (actually corotating streams emanating from coronal holes; for more details, see *Richardson et al.* [2000]), CME-related flows, and slow solar wind. Using mainly the measured

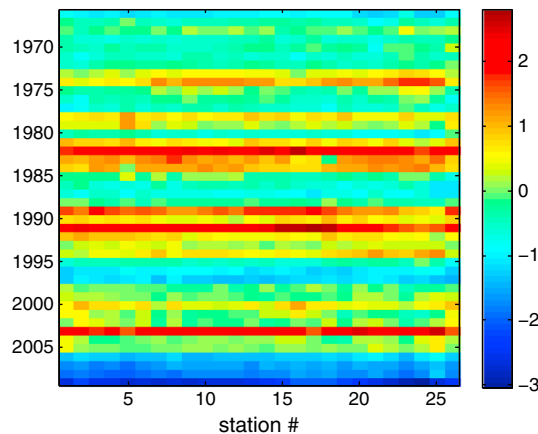


Figure 3. Data matrix of A_{hs} (standardized A_h) indices at 26 stations.

solar wind parameters included in the OMNI database (<http://omniweb.gsfc.nasa.gov/>), they have compiled a list, where the solar wind for each hour is assigned to one of the three types. The high-speed streams are identified as periods when the solar wind speed increases above ~ 450 km/s in about 1 day and decreases slowly during several days. Structures related to CME flows include not only the cores of interplanetary CMEs but also the associated upstream shocks and sheath regions. Because of data gaps in the OMNI database (particularly frequent in 1982–1994), there are some gaps in Richardson’s list (see Figure 2 which shows the yearly fractions of gaps).

4. Principal Component Analysis

4.1. Principal Component Analysis Method

In search for possible latitudinal patterns in the A_h indices we use the principal component analysis (PCA) method (for a review, see, e.g., *Hannachi et al.*, [2007]). In simple terms, PCA is a method which can be used to present a large number of partly correlated variables in terms of a smaller number of uncorrelated variables, called the *principal components*. The standardized annual means of the A_h indices of the 26 stations in 1966–2009 (44 values) are collected into a 44×26 data matrix (X) which is shown in color code in Figure 3. The stations are ordered by their corrected geomagnetic latitude (increasing from left to right) and they are numbered from 1 to 26 (see also Table 1). One can see that the columns in the data matrix are quite similar with each other, because all stations observe roughly the same solar cycle variation of geomagnetic activity. However, some small but systematic differences are seen in Figure 3, e.g., between the stations at low latitudes and auroral latitudes (compare, e.g., stations #1–5 and #19–25 in 1974 and 1994).

Principal component analysis uses the singular value decomposition of X

$$X = UDV^T \tag{2}$$

where U and V are orthogonal matrices ($UU^T = I$ and $VV^T = I$) and $D = \text{diag}(\lambda_1, \lambda_2, \dots, \lambda_{26})$ contains the singular values of the matrix X . The column vectors of the 26×26 matrix V are called the empirical orthogonal functions (EOFs). The principal components, which are uncorrelated with each other, are obtained as the column vectors of the 44×26 matrix

$$P = UD. \tag{3}$$

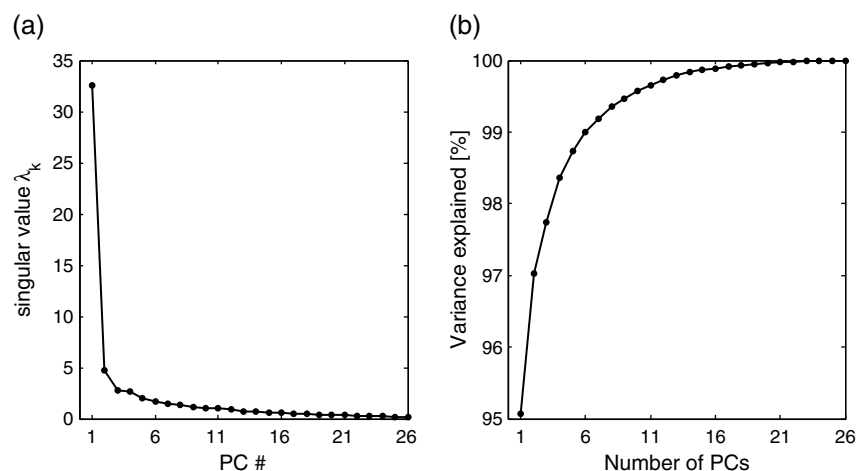


Figure 4. (a) Singular values λ_k of the data matrix. (b) Percentage of variance explained when increasing the number of principal components.

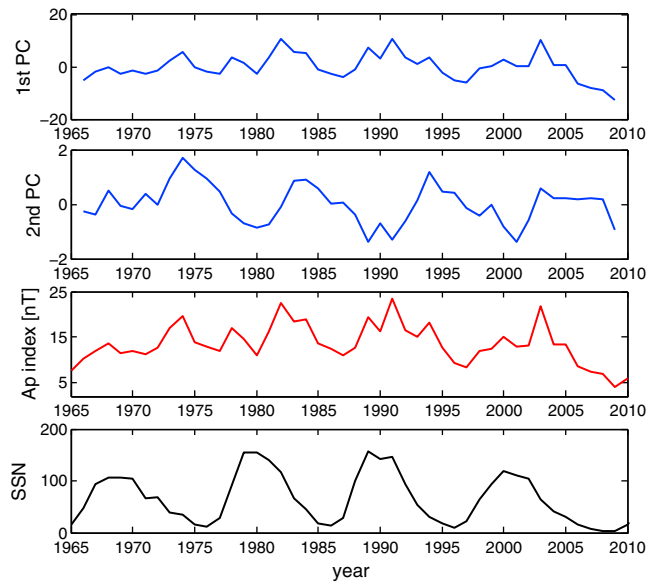


Figure 5. (top to bottom) The two first principal components, the Ap index, and the sunspot number, all at annual resolution.

The original variables can be now approximated using the K first principal components and EOFs as

$$X_{ij} = \sum_{k=1}^K P_{ik} V_{jk} \tag{4}$$

where X_{ij} is the value (A_{hs} index) of the j th variable (station) at the observation time (year) i .

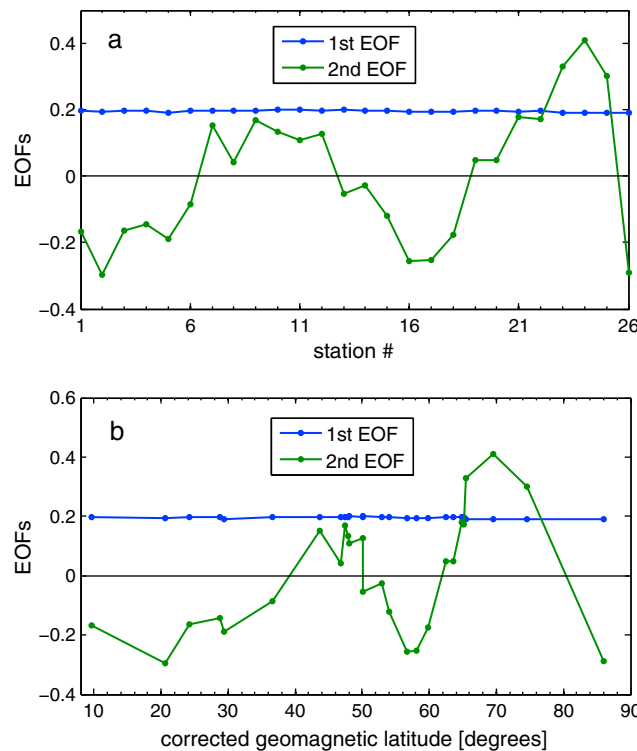


Figure 6. Two first EOFs as a function of (a) the station number and (b) the corrected geomagnetic latitude.

The variance of the k th PC is proportional to λ_k^2 . Hence, the K first PCs “explain” a percentage

$$\frac{\sum_{k=1}^K \lambda_k^2}{\sum_{k=1}^{26} \lambda_k^2} \cdot 100\% \tag{5}$$

of the variance in the original variables. The singular values of the data matrix X are plotted in Figure 4a. Clearly, the majority of variance in the data is explained by the first PC. The second singular value is much smaller than the first one, but it is still distinctly larger than the remaining singular values. This suggests that the second PC contains a physically meaningful signal. The other, smaller singular values and the respective PCs are neglected in this analysis. Figure 4b shows the percentage of variance explained when the number of PCs is increased. The first two PCs already contain 97.1% of the total variance in the data.

4.2. Two First Principal Components

Figure 5 shows the two first principal components of the A_{hs} indices in

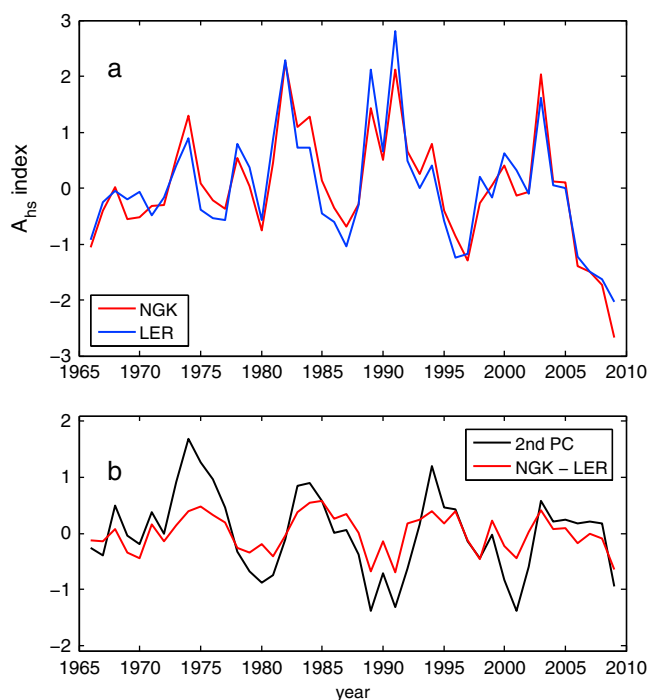


Figure 7. (a) Standardized A_{hs} indices at Lerwick (LER) and Niemegek (NGK) stations, and (b) their difference compared with the second PC.

meaning that the variation described by the second PC can be opposite in some stations included in the present network. The second PC does not contribute much to stations with small EOF values (such as stations #13 and 14), but the contribution can also be quite large for some stations (especially stations #23–25). Figure 6b shows the second EOF as a function of corrected geomagnetic latitude. The latitudinal variation of the second EOF is rather curious. High positive EOF values are found at stations #21–25 at auroral latitudes (65° – 75°). Interestingly, subauroral stations #15–18 (54° – 60°) depict negative values with a local minimum at about 57° – 58° , while midlatitude stations #7–12 (44° ... 50°) show again positive values with a local maximum at about 47° – 48° . Low-latitude stations #1–5 and the polar cap station #26 show negative values roughly equal with those at subauroral stations.

As an example of the difference between two stations, Figure 7a shows the A_{hs} indices of NGK (#10) and LER (#17), for which the second EOF attains opposite values. Both of these stations are also included in the network of stations used in calculating the Kp/Ap index. It is seen that although the A_{hs} indices at the two stations follow each other fairly closely over the whole 44 year time interval, there are times when their mutual differences are quite large.

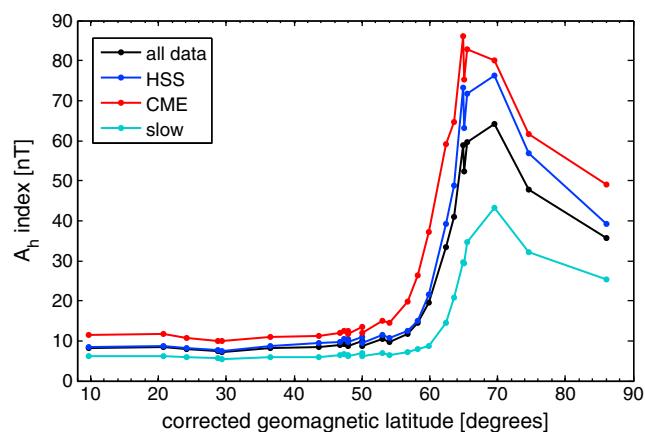


Figure 8. Averages of A_h indices during the three solar wind types.

1966–2009. Because of the overwhelming weight of the first PC, it practically agrees with the average of the 26 A_{hs} indices. This can also be seen from the first EOF depicted in Figure 6 which describes a “flat” latitudinal mode in which all stations have almost the same EOF value of about 0.2. This is also the reason why the first PC correlates almost perfectly (correlation coefficient = 0.99 and p value = $9.9 \cdot 10^{-34}$) with the annual Ap index which is also shown in Figure 5. In fact, the excellent mutual agreement of these two global parameters also supports the similarity of the A_h and K/Ak indices [Mursula and Martini, 2007b] and the sufficient global representation of the Ap index.

The second PC is the leading “correction term” which describes the most important common mode by which the 26 index series depart from their average described by the first PC. The EOF associated to the second PC (Figure 6a) has both negative and positive values,

meaning that the variation described by the second PC can be opposite in some stations included in the present network. The second PC does not contribute much to stations with small EOF values (such as stations #13 and 14), but the contribution can also be quite large for some stations (especially stations #23–25). Figure 6b shows the second EOF as a function of corrected geomagnetic latitude. The latitudinal variation of the second EOF is rather curious. High positive EOF values are found at stations #21–25 at auroral latitudes (65° – 75°). Interestingly, subauroral stations #15–18 (54° – 60°) depict negative values with a local minimum at about 57° – 58° , while midlatitude stations #7–12 (44° ... 50°) show again positive values with a local maximum at about 47° – 48° . Low-latitude stations #1–5 and the polar cap station #26 show negative values roughly equal with those at subauroral stations.

As an example of the difference between two stations, Figure 7a shows the A_{hs} indices of NGK (#10) and LER (#17), for which the second EOF attains opposite values. Both of these stations are also included in the network of stations used in calculating the Kp/Ap index. It is seen that although the A_{hs} indices at the two stations follow each other fairly closely over the whole 44 year time interval, there are times when their mutual differences are quite large. Figure 7b depicts these differences explicitly and shows that they are quite well explained by the second PC, which is also shown in Figure 7b. Note that the total weight of the second PC in the NGK-LER difference is only about 0.4 (see Figure 6a). This explains the smaller amplitude of the variations in this difference in Figure 7b compared to the second PC.

4.3. Second PC and Solar Wind Structures

Figure 5 shows that the second PC has a clear solar cycle variation with

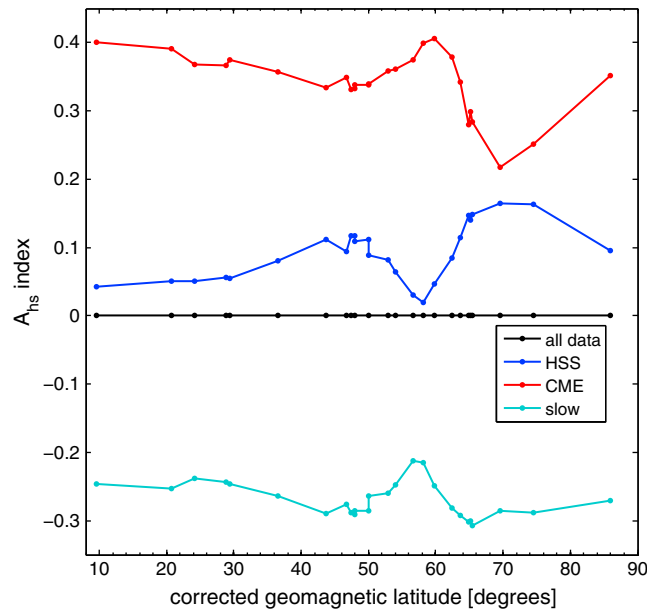


Figure 9. Averages of standardized A_{hs} indices during the three solar wind types.

the subauroral latitudes. Slow SW has its maximum at the highest auroral latitudes, which is roughly 5 times the mean level at midlatitudes and low latitudes. Figure 9 depicts the average values of the A_{hs} indices during each solar wind type. Note the striking similarity between the latitudinal distribution of the A_{hs} indices during HSSs and the second EOF depicted in Figure 6. This gives strong additional support for the result that the mode described by the second PC is indeed related to high-speed streams. Note also that the distributions of A_{hs} indices for HSSs and CMEs depict a clear overall anticorrelation ($cc = -0.92$), which is a natural consequence of the relatively small latitudinal variation of A_{hs} indices during slow SW.

The above results thus suggest that the second PC depends on the relative occurrence of HSSs in the solar wind. Figure 10 shows the yearly fractions of the three solar wind structures (CME, HSS, and slow SW). One can see the well-known fact that CME occurrence rate roughly follows the sunspot cycle, while the HSSs

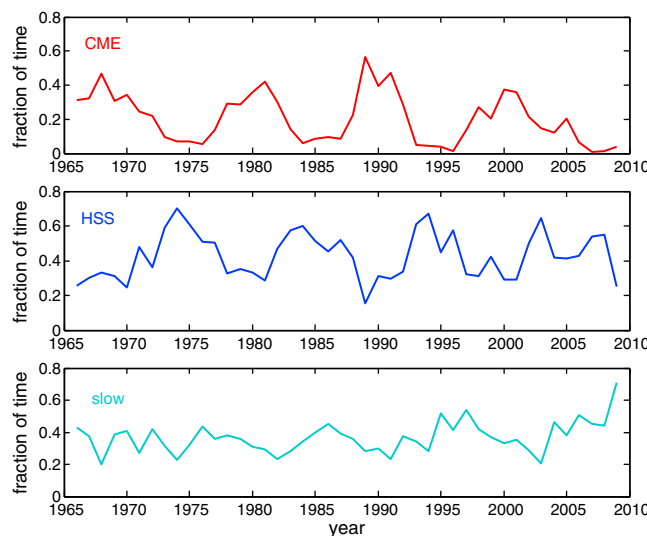


Figure 10. Yearly fractions of (top) CMEs, (middle) HSSs, and (bottom) slow solar wind.

dominate the solar wind during the declining phase and sunspot minima. The highest yearly fraction of HSSs in the satellite era occurred in 1974 when corotating high-speed streams were almost continuously present [see, e.g., Gosling *et al.*, 1976]. Slow SW attains its largest fractions around sunspot minima. The extraordinary minimum (2007–2009) of solar cycle 23 was exceptional also in terms of the solar wind structures. In 2007–2008 the CME fraction was almost zero, and in 2009 the fraction of slow solar wind was exceptionally large (about 70%). (For a detailed review of the solar wind flow types and their properties, see Richardson and Cane [2012]).

Figure 11 repeats the annual HSS fraction of Figure 10 and compares it

maxima in the late declining phase of the solar cycle and minima close to solar maxima. This suggests that the second PC is related to high-speed solar wind streams which typically are seen at 1 AU during the late declining phase. To test this hypothesis, we have depicted the averages of the A_h indices during the three different solar wind types in Figure 8. (Those time intervals when the solar wind type was unknown or any of the stations missed the 3 h A_h index were discarded). Figure 8 shows that at all stations CMEs produce the greatest average activity, far above the mean level. HSSs produce overall smaller average activity which is almost as strong as CMEs at the highest auroral latitudes (around 70°), but clearly smaller at lower latitudes, approaching the mean activity level below

the declining phase and sunspot minima. The highest yearly fraction of HSSs in the satellite era occurred in 1974 when corotating high-speed streams were almost continuously present [see, e.g., Gosling *et al.*, 1976]. Slow SW attains its largest fractions around sunspot minima. The extraordinary minimum (2007–2009) of solar cycle 23 was exceptional also in terms of the solar wind structures. In 2007–2008 the CME fraction was almost zero, and in 2009 the fraction of slow solar wind was exceptionally large (about 70%). (For a detailed review of the solar wind flow types and their properties, see Richardson and Cane [2012]).

Figure 11 repeats the annual HSS fraction of Figure 10 and compares it

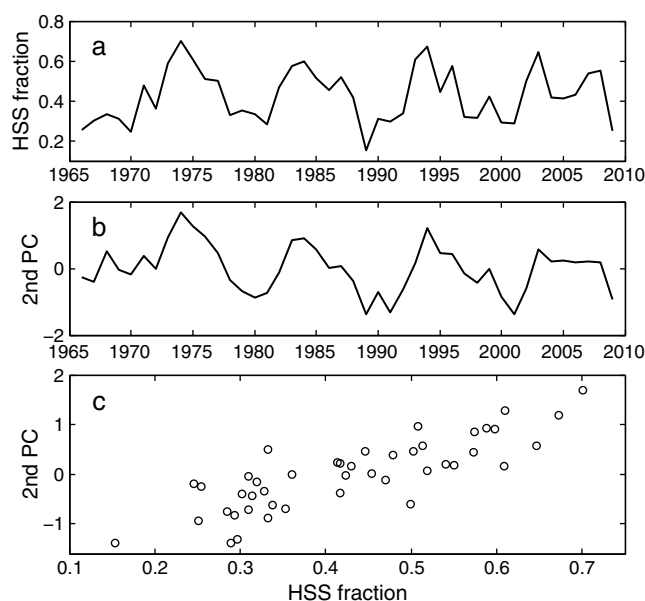


Figure 11. (a) Yearly fraction of time covered by high-speed streams in solar wind, (b) the second PC, and (c) scatterplot of the second PC as a function the yearly fraction of high-speed streams.

with the second PC. One can see that the second PC follows remarkably well the solar cycle variation of the annual fraction of HSS streams. The correlation coefficient between the two parameters is 0.83 (p value = $4.5 \cdot 10^{-12}$). This further supports the view that the second PC is related to high-speed streams. As expected, the highest second PC value is also found in 1974. Also the second highest second PC value in 1994 coincides with the second highest value of the HSS fraction. Naturally, there are some detailed differences between the two curves, for example, the third highest maximum of the HSS fraction in 2003 is underestimated by the second PC. This is probably due to the exceptionally strong CMEs in 2003 which tend to diminish the relative contribution of the frequent HSSs in that year. This interpretation is supported by the fact that the fraction of CMEs was

larger in 2003 than in other HSS maximum years 1974, 1984, and 1994 (see Figure 10).

5. Discussion

5.1. Other Possible Causes of the Second PC

It is known [Finch *et al.*, 2008] that there are latitudinal differences in the correlation between local geomagnetic activity and solar wind parameters. Finch *et al.* [2008] showed that the correlation between geomagnetic activity and solar wind speed maximizes around 70° geomagnetic latitude, i.e., at the poleward edge of the auroral region. This leads to the following question: does the solar wind speed determine

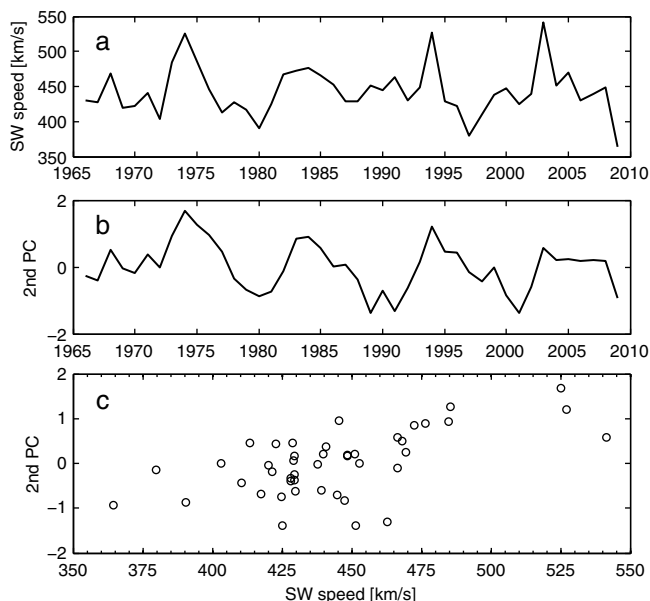


Figure 12. (a) Annual means of solar wind speed, (b) second PC, and (c) scatterplot of the second PC as a function of solar wind speed.

the latitudinal distribution of geomagnetic activity (depicted by the second PC)? Figure 12 depicts the second PC and the annual solar wind speed, which have a fair correlation (c.c. = 0.59, $p = 2.3 \cdot 10^{-5}$). (This is mainly determined by the three high values of $V_{SW} > 500$ km/s; without these 3 years the correlation is essentially weaker with $cc = 0.46$ and $p = 0.0023$). However, correlation of second PC with V_{SW} is considerably lower than with HSS fraction ($cc = 0.83$; $p = 4.5 \cdot 10^{-12}$), which can be understood as follows. During sunspot maximum years, when the CME fraction is high, the second PC is low (negative), but the solar wind speed is not necessarily low. For example, in 1989–1991 the solar wind was occupied by CMEs about 50% of the time (Figure 10), but the average solar wind speed was as high as about 450 km/s, i.e., close to the long-term average. However, during

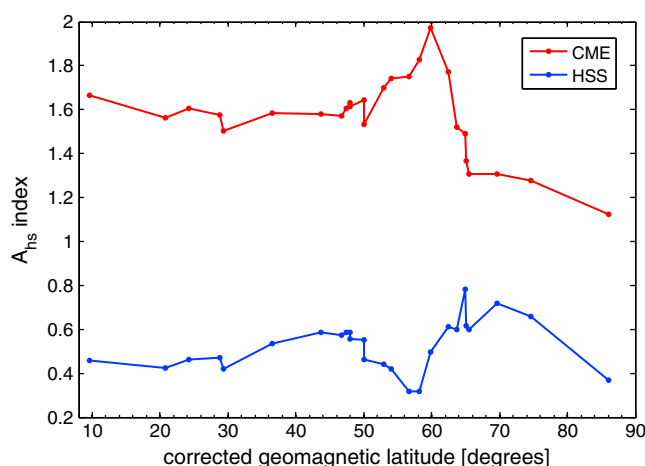


Figure 13. Averages of standardized A_{hs} indices during CME- and HSS-related substorms in 1980–2009.

the same years the second PC had a minimum since the HSS fraction was only about 15–30% (see Figure 10). The same situation occurs during the next sunspot maximum in 2000–2001. Accordingly, since CMEs can also include fairly high solar wind speeds, the value of SW speed alone does not explain the second PC as well as the HSS fraction. (Note also that the correlation between the second PC and HSS fraction depicted in Figure 11c remains high with $cc = 0.78$ and $p = 2.6 \cdot 10^{-9}$ even if the three highest fractions are removed.)

We note that, similar to the solar wind speed, no other “coupling function” (combination of solar wind speed,

interplanetary magnetic field B , or its rectified southward component B_S) provides a better correlation with the second PC than the HSS fraction. On the other hand, several coupling functions correlate extremely well with the global geomagnetic activity, and therefore, with the first PC. For example, there is an excellent correlation between the annual means of the aa index and BV^2 [Lockwood *et al.*, 2009]. Moreover, it has been noted [Richardson *et al.*, 2002; Richardson and Cane, 2012] that the linear relation between $B_S V^2$ and the aa index is roughly the same for all the three solar wind types (CME, HSS, and slow SW). Thus, the same coupling function explains the global geomagnetic activity (as measured by the aa index, or, e.g., the first PC) during all solar wind structures. However, the coupling functions do not explain well the latitudinal distribution of geomagnetic activity.

Calculation of the A_h (and all other K method-based) indices requires removing the quiet daily (Sq) variation from the H component when determining the 3 h range. Since the Sq variation cannot be perfectly removed from the data, a small contribution from the Sq variation will remain in the A_h indices. However, the residual Sq variation has no significant effect on the results of the PC analysis. We have tested this by repeating the above described PC analysis with local IHV indices [Svalgaard and Cliver, 2007]. The IHV indices are calculated by using data from the night sector only, thus being hardly affected by the Sq variation at all. When using the local IHV indices for the same stations, we get very similar first and second PCs and EOFs (not shown), and the second PC correlates again very well with the HSS fraction ($cc = 0.79$, $p = 1.2 \cdot 10^{-10}$). This shows that neither the temporal variation of the second PC nor the observed latitudinal structure of the second EOF is caused by the residual Sq variation in the A_h indices.

5.2. Latitudinal Variation of the Second EOF

There is a natural explanation why the HSS fraction explains the second PC and the latitudinal variation of the second EOF. As already mentioned in section 1, a large annual HSS fraction implies frequent substorm activity but a small number of intense storms. A large CME fraction in turn implies relatively larger number of strong storms that include substorms with a larger latitudinal extent. In the following we discuss the latitudinal distribution of the second EOF and its relation to the latitudinal differences between CME- and HSS-related disturbances.

The second EOF is negative for low-latitude stations #1–6 (Figure 6). This is because the ring current (stronger during CME storms than during HSS storms) has a great influence at low latitudes. The second EOF is positive for most stations at midlatitudes to auroral latitudes (#7–25). However, the most distinctive feature in Figure 6 are the negative values of the second EOF at subauroral latitudes of 50° – 60° (stations #13–18), with a minimum at about 57° – 58° . This is because the relative effect of CMEs is largest at these latitudes, reflecting the different behavior of auroral electrojets during CME- and HSS-related substorms. It is well known that under the influence of an intense solar wind electric field (especially in storm times) the polar cap and the auroral oval expand toward the equator and, consequently, substorm onsets (largest

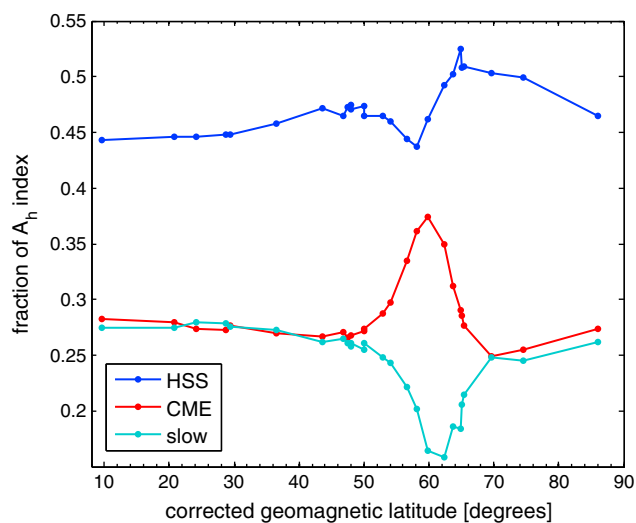


Figure 14. Fractions of the average A_h index produced by the three solar wind types.

disturbances during a substorm) occur at lower latitudes than under a weaker electric field [Hoffman *et al.*, 2010]. Since the average solar wind electric field during CMEs is stronger than during HSSs, it is expected that CME substorms occur at lower latitudes than HSS substorms, thus leading to the fact that the relative contribution of CMEs is larger at subauroral stations than at other stations. At midlatitudes of about 40° – 50° , where the CME-related electrojets no longer typically extend, the relative fraction of CMEs is reduced and the second EOF attains weakly positive values. On the other hand, the negative second EOF value of station #26 in the polar cap is most likely due to a significant contribution of the DP2 current, which is also

controlled by the solar wind electric field [Troshichev *et al.*, 1988] and, hence, is stronger during CMEs.

In order to verify the idea that CME substorms produce the subauroral minimum in the second EOF, we have plotted the averages of the A_{hs} indices during CME- and HSS-related substorms in Figure 13. We use the list of substorms identified by the SuperMAG magnetometer network (<http://supermag.uib.no/>) in 1980–2009 [Gjerloev, 2012]. The substorms are divided into CME (8083 substorms) and HSS-related (16734) substorms. Figure 13 shows that, on an average, CME substorms are observed to be relatively strongest at about 60° CGM latitude. On the other hand, the distribution during HSS substorms resembles the second EOF with a high maximum at auroral latitudes and a minimum at subauroral latitudes of about 57° – 58° .

The special importance of CMEs for geomagnetic activity at subauroral latitudes is further demonstrated in Figure 14 which depicts the fractions by which the three different solar wind types contribute to the average A_h indices at different stations. The contribution of the solar wind type i is calculated as $f_i \cdot \langle A_h \rangle_i / \langle A_h \rangle$, where $\langle A_h \rangle_i$ is the average level of the (nonstandardized) A_h index at given station during the SW type i , $\langle A_h \rangle$ the average A_h including all data and f_i the average fraction of time attained by the SW type (0.42 for HSSs, 0.20 for CMEs, and 0.37 for slow SW). Figure 14 also shows the basic fact that at all stations the majority of geomagnetic activity is produced by HSSs, although CMEs produce the highest momentary levels of geomagnetic activity (Figure 8).

6. Conclusions

In this paper, we have used the principal component analysis method to study the latitudinal distribution of geomagnetic activity measured by the local A_h indices of 26 stations in 1966–2009. We found that the temporal and latitudinal distribution of geomagnetic activity is very closely (up to about 97.1% of total variance) described by the first two principal components. The first PC closely agrees with the average of the 26 stations and describes the solar cycle variation of geomagnetic activity. It also correlates almost perfectly with indices of global geomagnetic activity, like the Kp/Ap index. The second PC, describing the leading pattern by which the latitudinal distribution of local geomagnetic activity deviates from the global average described by the first PC, was found to be strongly correlated with the (annual) time fraction of high-speed streams in solar wind. In fact, the second PC quantifies the difference in the latitudinal distribution of the relative disturbances associated with various current systems (in particular, the auroral electrojets and the ring current) between CMEs and HSSs.

The second EOF, the latitudinal mode associated with the second PC, was found to correspond to the average latitudinal distribution of the standardized A_h indices during high-speed streams and the total fraction of HSSs in the A_h indices. It has a high maximum at auroral latitudes, a local minimum at subauroral latitudes, and a low maximum at midlatitudes. The subauroral minimum in the second EOF was shown to be related

to the fact that CME-driven substorms occur, on an average, at lower latitudes than HSS-driven substorms, raising the relative significance of CMEs at the subauroral stations.

Finally, we note that the results presented in this study are very useful for long-term (space climate) studies, offering a method that can be used to gain information about the relative fraction of the statistical occurrence of various solar wind structures before the satellite era at annual resolution. While the present results are not directly available for event-based studies of solar wind structures, it may be possible to develop related methods based on techniques similar to those presented here.

Acknowledgments

We acknowledge the financial support by the Academy of Finland to the ReSolVE Center of Excellence (project 272157) and to project 264994. This work has benefited for collaborations and contacts within the COST ES1005 (TOSCA) Network Action (especially Working Group 2). The hourly magnetometer data were obtained from the World Data Center for Geomagnetism, Edinburgh (<http://www.wdc.bgs.ac.uk/>). The A_p index was obtained from World Data Center for Geomagnetism, Kyoto (<http://wdc.kugi.kyoto-u.ac.jp/>). The sunspot data were obtained from WDC-SILSO, Royal Observatory of Belgium, Brussels (<http://sidc.be/silso/>). The hourly values of the solar wind speed were obtained from the OMNI database (<http://omniweb.gsfc.nasa.gov/>). We thank Jesper W. Gjerloev for the SuperMAG-based list of substorms which is available at the SuperMAG website <http://supermag.uib.no/>. The list of the solar wind structures can be obtained by contacting Ian G. Richardson.

Michael Liemohn thanks the reviewers for their assistance in evaluating this paper.

References

- Bartels, J., N. H. Heck, and H. F. Johnston (1939), The three-hour-range index measuring geomagnetic activity, *Terr. Magn. Atmos. Electr.*, *44*, 411–454, doi:10.1029/TE044i004p00411.
- Belcher, J. W., and L. Davis (1971), Large-amplitude Alfvén waves in the interplanetary medium, *J. Geophys. Res.*, *76*(16), 3534–3563, doi:10.1029/JA076i016p03534.
- Borovsky, J. E., and M. H. Denton (2006), Differences between CME-driven storms and CIR-driven storms, *J. Geophys. Res.*, *111*, A07S08, doi:10.1029/2005JA011447.
- Echer, E., B. T. Tsurutani, and W. D. Gonzalez (2013), Interplanetary origins of moderate ($-100\text{ nT} < \text{Dst} \leq -50\text{ nT}$) geomagnetic storms during solar cycle 23 (1996–2008), *J. Geophys. Res. Space Physics*, *118*, 385–392, doi:10.1029/2012JA018086.
- Feynman, J. (1982), Geomagnetic and solar wind cycles: 1900–1975, *J. Geophys. Res.*, *87*(A8), 6153–6162.
- Finch, I. D., M. L. Lockwood, and A. P. Rouillard (2008), Effects of solar wind magnetosphere coupling recorded at different geomagnetic latitudes: Separation of directly-driven and storage/release systems, *Geophys. Res. Lett.*, *35*, L21105, doi:10.1029/2008GL035399.
- GFZ Potsdam (2012). [Available at http://www-app3.gfz-potsdam.de/kp_index/index.html]
- Gjerloev, J. W. (2012), The SuperMAG data processing technique, *J. Geophys. Res.*, *117*, A09213, doi:10.1029/2012JA017683.
- Gosling, J. T., J. R. Asbridge, S. J. Bame, and W. C. Feldman (1976), Solar wind speed variations: 1962–1974, *J. Geophys. Res.*, *81*, 5061–5070.
- Hannachi, A., I. T. Jolliffe, and D. B. Stephenson (2007), Empirical orthogonal functions and related techniques in atmospheric science: A review, *Int. J. Climatol.*, *27*, 1119–1152, doi:10.1002/joc.1499.
- Hoffman, R. A., J. W. Gjerloev, L. A. Frank, and J. W. Sigwarth (2010), Are there optical differences between storm-time substorms and isolated substorms?, *Ann. Geophys.*, *28*(5), 1183–1198, doi:10.5194/angeo-28-1183-2010.
- IGRF (2010), International Geomagnetic Reference Field, the International Association of Geomagnetism and Aeronomy (IAGA). [Available at <http://www.ngdc.noaa.gov/AGA/vmod/index.html>]
- Karinen, A., and K. Mursula (2005), A new reconstruction of the Dst index for 1932–2002, *Ann. Geophys.*, *23*, 475–485.
- Lockwood, M., A. P. Rouillard, and I. D. Finch (2009), The rise and fall of open solar flux during the current grand solar maximum, *Astrophys. J.*, *700*, 937–944, doi:10.1088/0004-637X/700/2/937.
- Martini, D., and K. Mursula (2008), Centennial geomagnetic activity studied by a new, reliable long-term index, *J. Atmos. Sol. Terr. Phys.*, *70*, 1074–1087, doi:10.1016/j.jastp.2008.01.008.
- Mayaud, P.-N. (1972), The aa indices: A 100-year series characterizing the magnetic activity, *J. Geophys. Res.*, *77*(34), 6870–6874.
- Mayaud, P. N. (1980), Derivation, meaning, and use of geomagnetic indices, *Geophys. Monogr. Ser.*, vol. 22, 607 pp., AGU, Washington, D. C., doi:10.1029/GM022.
- Menvielle, M., and A. Berthelier (1991), The K-derived planetary indices—Description and availability, *Rev. Geophys.*, *29*, 415–432, doi:10.1029/91RG00994.
- Mursula, K., and D. Martini (2007a), A new verifiable measure of centennial geomagnetic activity: Modifying the K index method for hourly data, *Geophys. Res. Lett.*, *34*, L22107, doi:10.1029/2007GL031123.
- Mursula, K., and D. Martini (2007b), New indices of geomagnetic activity at test: Comparing the correlation of the analogue a_k index with the digital A_p and IHV indices at the Sodankylä station, *Adv. Space Res.*, *40*, 1105–1111, doi:10.1016/j.asr.2007.06.067.
- Newell, P. T., and J. W. Gjerloev (2012), SuperMAG-based partial ring current indices, *J. Geophys. Res.*, *117*, A05215, doi:10.1029/2012JA017586.
- Richardson, I. G., and H. V. Cane (2012), Near-earth solar wind flows and related geomagnetic activity during more than four solar cycles (1963–2011), *J. Space Weather Space Clim.*, *2*(26), A02, doi:10.1051/swsc/2012003.
- Richardson, I. G., E. W. Cliver, and H. V. Cane (2000), Sources of geomagnetic activity over the solar cycle: Relative importance of coronal mass ejections, high-speed streams, and slow solar wind, *J. Geophys. Res.*, *105*, 18,203–18,214, doi:10.1029/1999JA000400.
- Richardson, I. G., H. V. Cane, and E. W. Cliver (2002), Sources of geomagnetic activity during nearly three solar cycles (1972–2000), *J. Geophys. Res.*, *107*, 1187, doi:10.1029/2001JA000504.
- Richardson, I. G., et al. (2006), Major geomagnetic storms ($\text{Dst} \leq -100\text{ nT}$) generated by corotating interaction regions, *J. Geophys. Res.*, *111*, A07S09, doi:10.1029/2005JA011476.
- Simon, P. A., and J. P. Legrand (1986), Some solar cycle phenomena related to the geomagnetic activity from 1868 to 1980. II. High velocity wind streams and cyclical behaviour of poloidal field, *Astron. Astrophys.*, *155*, 227–236.
- Svalgaard, L., and E. W. Cliver (2007), Interhourly variability index of geomagnetic activity and its use in deriving the long-term variation of solar wind speed, *J. Geophys. Res.*, *112*, A10111, doi:10.1029/2007JA012437.
- Tanskanen, E. I., J. A. Slavin, A. J. Tanskanen, A. Viljanen, T. I. Pulkkinen, H. E. J. Koskinen, A. Pulkkinen, and J. Eastwood (2005), Magnetospheric substorms are strongly modulated by interplanetary high-speed streams, *Geophys. Res. Lett.*, *32*, L16104, doi:10.1029/2005GL023318.
- Troshichev, O. A., V. G. Andrezen, S. Vennerstroem, and E. Friis-Christensen (1988), Magnetic activity in the Polar Cap—A new index, *Planet. Space Sci.*, *36*, 1095–1102.
- Tsurutani, B. T., et al. (2006), Corotating solar wind streams and recurrent geomagnetic activity: A review, *J. Geophys. Res.*, *111*, A07S01, doi:10.1029/2005JA011273.
- WDC-C1 (2011), World Data Center for Geomagnetism, Edinburgh, U. K. [Available at <http://www.wdc.bgs.ac.uk/>]
- Yakovchouk, O. S., K. Mursula, L. Holappa, I. S. Veselovsky, and A. Karinen (2012), Average properties of geomagnetic storms in 1932–2009, *J. Geophys. Res.*, *117*, A03201, doi:10.1029/2011JA017093.
- Zhang, J., et al. (2007), Solar and interplanetary sources of major geomagnetic storms ($\text{Dst} < -100\text{ nT}$) during 1996–2005, *J. Geophys. Res.*, *112*, A10102, doi:10.1029/2007JA012321.